# A geochemical model for the transformation of gabbro into vesuvianite-bearing rodingite

Juraj Butek, Sébastien Fabre, Stéphanie Duchene, Ján Spišiak, Michel Grégoire

# A geochemical model for the transformation of gabbro into vesuvianite-bearing rodingite

Juraj Butek[1], Sébastien Fabre[2], Stéphanie Duchene[3], Ján Spišiak[1], Michel Grégoire[3]

[1]*Faculty of Natural Sciences, Matej Bel University, Tajovského 40, 97401 Banská Bystrica, Slovakia; juraj.butek@umb.sk*

[2]*Institut de Recherche en Astrophysique et Planétologie (IRAP), CNRS, UPS, Observatoire Midi-Pyrénées (OMP), 14 Av. E. Belin, 31400 Toulouse, France*

[3]*Géosciences Environnement Toulouse (GET), CNRS, UPS, IRD, CNES, Université de Toulouse, Observatoire Midi-Pyrénées (OMP), 14 Av. E. Belin, 31400 Toulouse, France*

## Abstract

Rodingite is a Ca-rich and Si-poor metasomatic rock commonly occurring in association with serpentinites. This rock is characterized by specific mineral assemblages consisting of hydrated garnet, diopside, vesuvianite, epidote-zoisite, chlorite, or prehnite. However, natural rodingites are significantly heterogeneous in mineral composition and vesuvianite occurs only in some extensively rodingitized rocks. Major factors controlling the mineral diversity as well as details on fluid-rock interactions leading to the evolution of mineral and chemical composition during rodingitization have not yet been fully constrained. In this work, we use PHREEQC software to present a geochemical model for the transformation of a mafic rock into vesuvianite-bearing rodingite at a temperature of 300°C. Through these simulations, we investigate the effect of fluid composition and progress of the metasomatic process on rodingite formation. Our results show that rodingitization requires an open system with a high input of hydrothermal fluid. Additionally, a decrease in the Si/Ca ratio in the metasomatized rock is correlated to an increase in the volume of incoming fluid. Whole rock chemical and mineral composition in natural rodingites are well reproduced by the model. Furthermore, the diversity of mineral parageneses results mainly from different degrees of transformation and only to a lesser extent to the chemical composition of hydrothermal fluid or protolith. The hydrothermal fluid doesn't need to be especially rich in calcium to transform a mafic rock into rodingite, but it must be low in magnesium, silicon, and have a high pH, which is naturally controlled by serpentinization of surrounding ultramafic rocks.

## 1 Introduction

Serpentinized ultramafic lithologies frequently contain bodies of a heterogeneous pale rock known as rodingite. Rodingite is a Ca-rich and Si-poor metasomatic rock typically consisting of hydrated garnet, diopside, chlorite, vesuvianite, epidote-zoisite, and prehnite (Coleman, 1967; Schandl et al., 1989; Li et al., 2004). Rodingites are most commonly interpreted to form by hydrothermal alteration of a gabbroic rock during concurrent serpentinization of surrounding ultramafic lithology (e.g. Li et al., 2004, 2017; Karkalis et al., 2022; Duan et al., 2022; Zhao et al., 2023; Xiong et al., 2024). The rodingitization process is characterized by significant changes in whole rock composition, namely Ca-enrichment and Si, Na and K leaching from the mafic protolith (Li et al., 2007, 2017; Koutsovitis et al., 2013; Tang et al., 2018; Laborda-López et al., 2020).

Rodingite mineral composition is generally very heterogeneous, even at a sample scale. Petrographic observations commonly allow the identification of paragenesis evolution during rodingitization, leading to systematic differences between the mineral composition of slightly rodingitized and extensively rodingitized samples. A lesser extent of metasomatic transformation is typically characterized by presence of prehnite, chlorite, epidote-clinozoisite, albite or tremolite (Schandl et al., 1989; Attoh et al., 2006; Li et al., 2017; Wang et al., 2019; Duan et al., 2021, 2022). In contrast,

extensively rodingitized rocks consist predominantly of hydrated garnet, diopside and vesuvianite (Li et al., 2004, 2007, 2008, 2017; Zanoni et al., 2016; Duan et al., 2022; Butek et al., 2022).

Rodingite can form under variable *P-T* conditions. Fluid inclusion studies indicate that the rodingitization process occurs at temperatures ranging from 250 to 400°C and pressures from 100 to 400 MPa (Schandl et al., 1989; Mittwede and Schandl, 1992; Dubińska et al., 2004; Normand and Williams-Jones, 2007), which presumably represent the most common conditions of rodingite formation (e.g. Koutsovitis et al., 2013). Rodingites occur on present-day ocean floor (Honnorez and Kirst, 1975; Frost et al., 2008) but are most commonly described from ophiolitic serpentinite occurrences around the world. However, the specific rodingite parageneses remain stable over a large range of pressures and temperatures, eventually recrystallizing at high P-T conditions to form "metarodingites" (Li et al., 2007, 2008; Zanoni et al., 2016; Laborda-López et al., 2018; Haws et al., 2021). Therefore, the possibility of rodingite formation at high pressure and temperature in subduction zone environments must be considered and the interpretation of the geodynamic setting of rodingite formation is thus still a subject of discussion (Ferrando et al., 2010; Hu and Santosh, 2018; Wang et al., 2019; Butek et al., 2023).

One of the first systematic investigation of the thermodynamic stability of rodingite parageneses was conducted by Rice (1983). Later, Palandri and Reed (2004) presented a comprehensive geochemical modeling study focusing on serpentinization, which included also some calculations to simulate the rodingitization process. Through the incremental dissolution of a gabbroic rock in a fixed amount of fluid obtained from equilibration with serpentinite, they successfully predicted the formation of minerals such as chlorite, vesuvianite, prehnite, diopside and garnet. They concluded that the rodingitization process is a result of Ca metasomatism driven by reducing, hyperalkaline, Ca-rich fluid produced during serpentinization. Other geochemical modeling studies investigating the rodingitization process in detail were also able to reproduce the rodingite paragenesis and pointed out the importance of silica leaching during the formation of rodingites (Frost and Beard, 2007; Frost et al., 2008; Bach and Klein, 2009; Bach et al., 2013). However, none of these models (Frost and Beard, 2007; Frost et al., 2008; Bach and Klein, 2009; Bach et al., 2013) included vesuvianite, despite the fact that this mineral represents a characteristic mineral phase of rodingite paragenesis abundant in extensively rodingitized rocks with whole rock composition significantly different from their mafic protolith (Li et al., 2004, 2007, 2008, 2017; Zanoni et al., 2016; Duan et al., 2022; Butek et al., 2022).

Recently, numerous successful attempts to determine P-T-x conditions of rodingite formation have been performed using thermodynamic modeling softwares such as Perple_X or Thermocalc (Li et al., 2008; Zanoni et al., 2016; Laborda-López et al., 2018; Duan et al., 2021, 2022). However, these softwares focus on reliably identifying thermodynamically stable phases at defined *P-T-x* conditions, but their capacity to specify the composition of hydrothermal fluid in equilibrium with solid component(s) remains limited.

In this work, for the first time to our knowledge, we explore the process of rodingitization using the geochemical thermodynamic modeling software PHREEQC (Parkhurst and Appelo, 2013). We aim to constrain the physicochemical conditions driving the transformation of a gabbroic protolith into rodingite and to explain the diversity of secondary minerals, more specifically the presence of vesuvianite, in the extensively rodingitized rocks. Five factors should be considered that possibly influence the stability of vesuvianite and therefore the conditions leading to the formation of vesuvianite-bearing rodingites: 1) initial rock composition, 2) initial fluid composition, 3) fluid amount in the system (or fluid-rock ratio), 4) temperature, and 5) pressure. Since gabbro represents the most common protolith of rodingites (1) and the rodingitization process occurs typically at (sub)greenschist-

facies conditions (4, 5), we focus our study on the effects of the chemical composition of the interacting fluid (2) and its amount in the hydrothermal system (3).

# 2 Methodology

## 2.1 Outline of the PHREEQC geochemical model

A series of calculations was performed to determine the conditions of fluid-rock interaction yielding the whole rock chemistry and mineralogical assemblages typical for rodingites using PHREEQC software 3.1.2 (Parkhurst and Appelo, 2013). The calculations were performed using PHREEQC's implementations of an extended Debye-Hückel "B-dot" equation to compute solute activities coefficients (Helgeson, 1969; Anderson, 2005), and as a Peng-Robinson equation to compute the gas fugacity coefficients (Peng and Robinson, 1976). Fluid-rock compositions were computed iteratively using a Newton-Raphson algorithm until all species present as solid and gases were supersaturated with respect to the speciated solution. Temperatures and pressures remained fixed throughout every calculation, but pH and redox (set as the electron potential $pe = -\log a_{e^-}$ where $a_{e^-}$ is the electron activity) were allowed to vary.

The thermodynamic database used in the calculations was issued from SupPhreeqc program (Zhang et al., 2020) converting the classic thermodynamic dataset from SUPCRTBL (Zimmer et al., 2016) into a format readable by PHREEQC. The database works reliably up to 300°C and calculates the pressure according to the $H_2O$ saturation curve, i.e. around 8.584 MPa at 300°C. The coherence of the calculations for reactions and gases behaviours at 300°C has been verified by the authors of the PHREEQC code (Appelo et al., 2014).

The fluid-rock interaction was modeled in a system Na-K-Ca-Fe-Mg-Al-Si-H-O-C-S-Cl. Other elements were not considered since they are not present in hydrothermal fluid in significant amounts, or they do not represent a key compound of rock-forming minerals of interest. Since there is no thermodynamic data available for vesuvianite solid solution or hydrated component in garnet, for consistency we considered all minerals as pure phases and no solid solution models were included in the model. We emphasize that the formula of vesuvianite implemented in the database ($Ca_{19}Mg_2Al_{11}Si_{18}O_{78}H_9$) does not include iron or other minor element, despite the fact that natural vesuvianite can incorporate significant amounts of various elements such as Ti, Mn, Cr, B or even Cu (Groat et al., 1992; Aksenov et al., 2016). Indeed, the absence of solid solutions could have a considerable effect on any divergence between natural and calculated systems.

A mineral phase named MHSH (magnesium-hydroxide-sulphate-hydrate) is missing in the thermodynamic database but it represents an important mineral precipitating from seawater fluid in ocean floor environments as demonstrated by experimental studies (Janecky and Seyfried, 1983). We thus incorporated the values for the hydrolysis constant (*K*) into the PHREEQC calculation script to complement the thermodynamic dataset. The hydrolysis constant for the MHSH is defined by the reaction $Mg_{1.25}O_5SH_{1.5} + 0.5\ H^+ = 1.25\ Mg^{2+} + SO_4^{2-} + H_2O$ and can be expressed by the equation:

$$K(T) = \frac{a_{Mg^{2+}}^{1.25} \times a_{SO_4^{2-}} \times a_{H_2O}}{a_{H^+}^{0.5}}$$

where *a* is the activity of corresponding component expressed in mol/kgw. Values for molal Gibbs free energy for the components were taken from SUPCRTBL (Zimmer et al., 2016). The effect of temperature on the hydrolysis constant was calculated on the water saturation curve by linear regression of values measured by Janecky and Seyfried (1983) and is expressed by the polynomial coefficients in the following equation:

$$\log K(T) = -386.007 - 0.109\,T + 15288.907\,T^{-1} + 150.598\log(T)$$

where *T* is the temperature expressed in kelvin.

## 2.2 Calculation setup

In the calculations, the initial rock was put in contact with the solution. If the solution was undersaturated, primary phases dissolved to reach chemical equilibrium. The chemical equilibrium is defined by the saturation index of zero and can be expressed by the equation:

$$log\frac{Q}{K(T)} = 0$$

with *Q* the ionic product and *K(T)* the equilibrium constant as function of temperature. If the solution was oversaturated with respect to a secondary mineral, i.e. its saturation index reached a positive value, it precipitated to maintain the chemical equilibrium. This dissolution-precipitation process allows to calculate a mass-balance for each element. Kinetic limitations were not considered so that all thermodynamically stable mineral phases were allowed to precipitate. In every calculation, we thus investigated only the final state (i.e. complete transformation) resulting from the chemical equilibrium.

Temperature was invariably set to 300°C. Pressure was computed in the models according to the $H_2O$ saturation curve and it is of note that the resulting values (8.584 MPa for 300°C) are low compared to natural hydrothermal systems. However, previous works have shown that changes in pressure do not drastically affect the mineral assemblage stability in rodingite (Li et al., 2008; Duan et al., 2022) and pressure can be thus regarded as a minor parameter. The initial rock was a gabbro, with a composition taken as an average from MacLeod et al. (2017), Fe-Ti gabbros excluded, of 51.97 $SiO_2$, 16.58 $Al_2O_3$, 12.84 CaO, 9.14 MgO, 6.38 FeO, 3.03 $Na_2O$ and 0.06 $K_2O$ (values in wt.%). The amount of solid phase was fixed at 1 kg while the amount of fluid varied between 10 and 1000 kg, i.e. the investigated range of fluid-rock ratio varied from 10 to 1000 (Fig. 1). By contrast, earlier fluid-rock interaction modeling studies (Palandri and Reed, 2004; Bach and Klein, 2009) considered a fixed amount of fluid and incremental addition of a rock amount. Our approach aimed to ease the evaluation of mineral and chemical changes in the rock since its amount remained constant in every calculation. Moreover, even though the increasing fluid amount can be seen as increasing fluid-rock ratio, we prefer to avoid using this expression. The concept of fluid-rock (or water-rock) ratio is commonly used in studies dedicated to fluid-rock interactions; however, its meaning is often ambiguous. In our case, the increasing amount of fluid in the system simply corresponds to an increase of the progress of transformation and can be thus correlated with reaction progress. In this sense, low fluid amount represents an onset of the metasomatic transformation and, on the other hand, very high fluid amounts represent an open hydrothermal system where an extremely high volume of fluid circulates during the metasomatic process. Such high fluid amounts thus represent an infinite-acting reservoir with a fluid of stable composition.

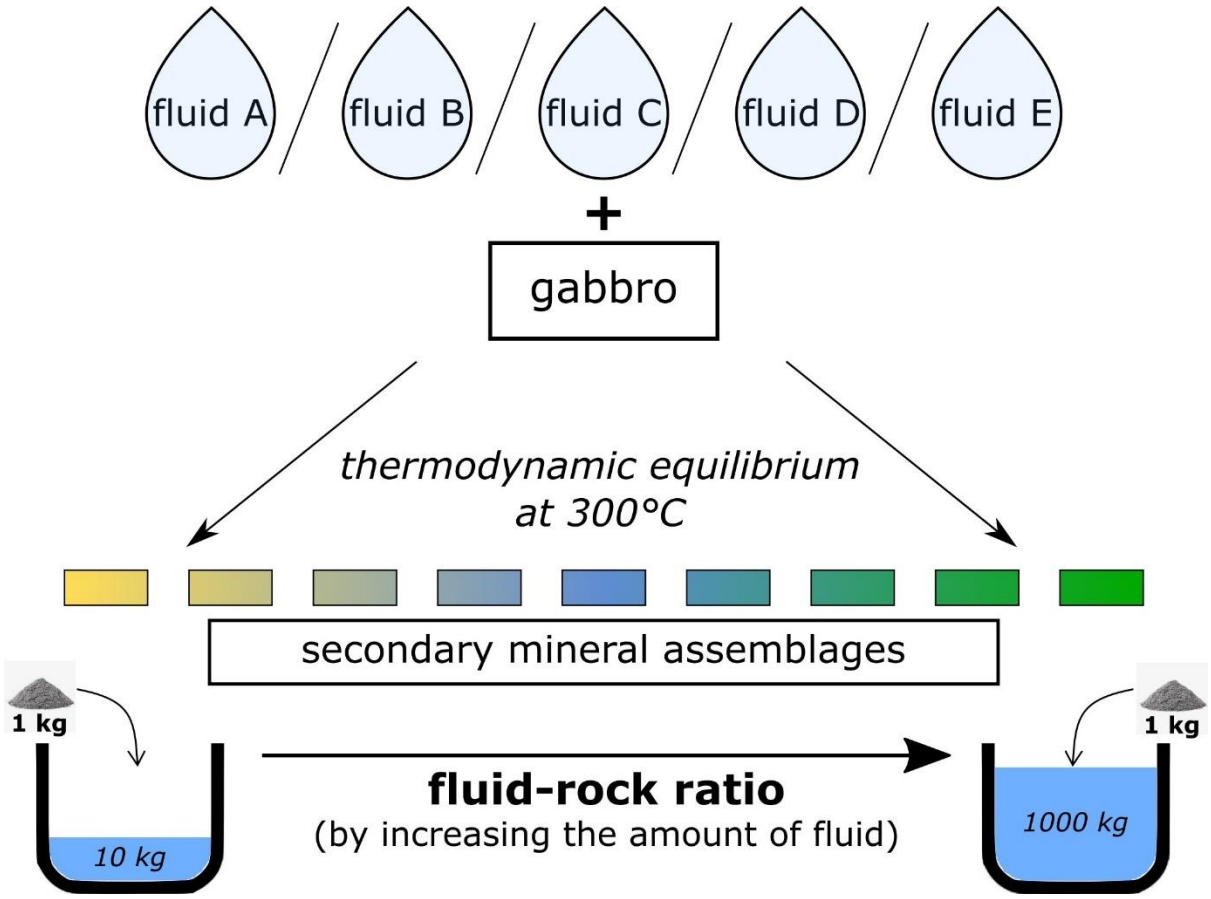


*Figure 1 Simple sketch illustrating the calculation setup. Hydrothermal fluids of different composition were set to react with a gabbro at 300°C. Please see the main text for the details on the fluid compositions used for the model calculations. Variable fluid-rock ratios were secured by increasing the amount of hydrothermal fluid, i.e. the mass amount of rock was constant (1 kg) while the mass amount of fluid varied between 10 and 1000 kg. Thermodynamic equilibrium was reached in the system by precipitating secondary mineral phases.*

## 2.3 Initial fluid compositions

Several fluid types (Tab 1) were considered in the calculations to test the influence of different chemical compositions on predicted mineral assemblages.

Model *A* simulates alteration with pure water.

Model *B* simulates alteration with an average seawater. The composition was taken from Nordstrom et al. (1979) and was simplified by removing minor and trace elements.

Model *C* simulates alteration with an evolved hydrothermal oceanic fluid, such as sampled at the Logatchev vent site (Charlou et al., 2002). The site is located at the Atlantic mid-ocean ridge (14°45'07.2"N 44°58'42.6"W) and its environment is dominated by ultramafic rock sequences. The fluid composition was measured directly at the vent opening and is thus considered a natural representative of fluids related to the serpentinization and rodingitization processes. This fluid is characterized by low pH (3.3) and is devoid of Mg and S. Compared to the seawater composition, it is about 3 times richer in Ca and more than 2 times richer in K. It is worth noting that the presence of $H_2$ (12 mmol/kg) and reduction conditions expressed with pe = -3.9. The concentration of Si (8.2 mmol/kg) is significantly higher than that in the seawater.

Model *D* simulates alteration with a fluid in equilibrium with serpentinite resulting from an experiment performed by Klein et al. (2015) during which a harzburgite sample was set to react with a hydrothermal fluid. The initial fluid used in the experiment represented a theoretical evolved seawater enriched in Ca and K (2-3 times) and completely devoid of Mg and S. The fluid composition was inspired by general knowledge that descending seawater leaches Ca and K from ocean floor basalts, and as a result of increasing temperature, secondary magnesium hydroxide sulphates (MHSH) and anhydrite precipitate and effectively remove Mg and S from the fluid (Mottl, 1983; Alt, 1995). After the reaction with harzburgite, the fluid's pH increased to 9 and was also characterized by a significant concentration of $H_2$ (7.7 mmol/kg). This is in good agreement with the high reducing potential commonly reported in serpentinization fluids (e.g. Barnes et al., 1978; Kelley et al., 2001).

*Table 1 Fluid compositions investigated in the models. A) pure water. B) average seawater (Nordstrom et al., 1979). C) evolved seawater composition measured in a vent at Logatchev (Charlou et al, 2002). D) experimental serpentinization fluid (Klein et al., 2015). E) experimental serpentinization fluid (Seyfried et al.,2007). Element concentrations are in mmol/kg.*

| | **A** | **B** | **C** | **D** | **E** |
|---|---|---|---|---|---|
| pH | 7 | 8.22 | 3.3 | 9 | 12.2 |
| pe | 4 | 8.451 | -3.9 | -9.5 | -13 |
| Ca | - | 10.66 | 27.3 | 27.6 | 8 |
| Mg | - | 55.09 | - | 0.06 | - |
| Na | - | 485.44 | 430 | 454.5 | 593 |
| K | - | 10.58 | 21.9 | 34.5 | 14 |
| Fe | - | 0.00004 | 2.5 | - | - |
| Si | - | 0.074 | 8.2 | 0.05 | 0.286 |
| Cl | - | 565.76 | 515 | - | 597 |
| Cl* | - | 566.6 | 512.1 | 544.3 | 584.7 |
| H(0) | - | - | 24 | 15.4 | 153.4 |
| S(6) | - | 29.26 | - | - | 5.3 |
| C(4) | - | 2.17 | 10.1 | - | - |

** adjusted to charge balance the solution*

Model *E* is similar to model *D* in the fact that the experimental solution reflects a composition measured after a serpentinization experiment (Seyfried et al., 2007). A seawater composition was used as the initial fluid for the experiment. The resulting serpentinization fluid is characterized by high pH (12.2) and very high concentration of dissolved $H_2$ (76.7 mmol/kg). Furthermore, Mg is completely removed from the fluid and $SO_4^{2-}$ is significantly depleted relative to the seawater composition. These values are also in good agreement with fluid compositions from ultramafic system–hosted hydrothermal vents measured in situ (e.g. Seyfried et al., 2015).

# 3 Results

## 3.1 Effect of the fluid amount on the mineral assemblage

The mineralogy resulting from fluid rock interaction is presented here for two values of fluid amount for each model: 1) 10 kg, simulating the first stage of metasomatic transformation), and 2) 1000 kg, simulating the final stage induced by extremely high amount of fluid.

At a low fluid amount (10 kg), the interaction of gabbro with pure water (model *A*) leads to a secondary assemblage consisting of albite (26.9 %), prehnite (21.2 %), tremolite (15.6 %), clinochlore (14.4 %), hedenbergite (4.1 %), daphnite (3 %) and stilpnomelane (2.9 %) (Fig. 2a). The interaction with seawater (model *B*) predicts epidote (32.6 %), clinochlore (23.9 %), tremolite (10.8 %), quartz (10.8 %), albite (10.5 %), wairakite (9.2 %) and anhydrite (2.1 %). A trace amount of pyrite (0.25 %) is also predicted but is not visible in the figure. In the model *C* using the natural hydrothermal fluid, the secondary assemblage consists of prehnite (35.2 %), tremolite (18.6 %), stilpnomelane (18.2 %), clinochlore (10.5 %), albite (10 %) and wairakite (7.4 %). The same phases (with slightly different proportions: 37.5 %, 18.3 %, 18 %, 11.1 %, 11.8 % and 3.3 %, respectively) are also predicted from the interaction with the first experimental serpentinization fluid (model *D*). The interaction of gabbro with the second experimental serpentinization fluid (model *E*) leads to a secondary assemblage consisting of albite (33.8 %), clinochlore (25.1 %), hedenbergite (16.9 %), prehnite (15.3 %), vesuvianite (8.4 %) and diopside (0.5 %). A trace amount of troilite (0.07 %) is also predicted but is not visible in the figure. We note that the only case where vesuvianite is predicted at low fluid amount is in model *E* (Fig. 2a).

On the other hand, at a high fluid amount (1000 kg), the interaction of gabbro with pure water (model *A*) leads to a secondary assemblage consisting of epidote (51.8 %), clinochlore (38.7 %) and vesuvianite (9.5 %) (Fig. 2b). A trace amount of clinozoisite (0.01 %) is also predicted but is not visible in the figure. The interaction with seawater (model *B*) predicts anhydrite (54.6 %), clinochlore (33.3 %), magnesium-hydroxide-sulphate-hydrate (10.4 %) and minor amounts of hematite (1.1 %) and talc (0.6 %). In model *C*, the secondary assemblage consists of daphnite (40.5 %), clinochlore (25.5 %), wairakite (16.9 %), quartz (9.8 %) and chloritoid (7.3 %). In the case of the experimental serpentinization fluid (model *D*), predicted phases are represented by epidote (47.7 %), clinochlore (35.8 %), vesuvianite (15.4 %) and clinozoisite (1.2 %). Finally, the interaction of gabbro with the second experimental serpentinization fluid (model *E*) leads to a secondary assemblage consisting of vesuvianite (56.1 %), monticellite (20.4 %), andradite (14 %) and wollastonite (9.3 %). A trace amount of rankinite (0.16 %) is also predicted but is not visible in the figure. At high fluid amount, vesuvianite is predicted in three of these models (compared to only one at low fluid amount) and on top of that, vesuvianite is the most dominant phase in the predicted assemblage in model *E* (Fig. 2b). Presence of vesuvianite in the calculated mineralogy is thus clearly favoured by high amount of fluid in the system.

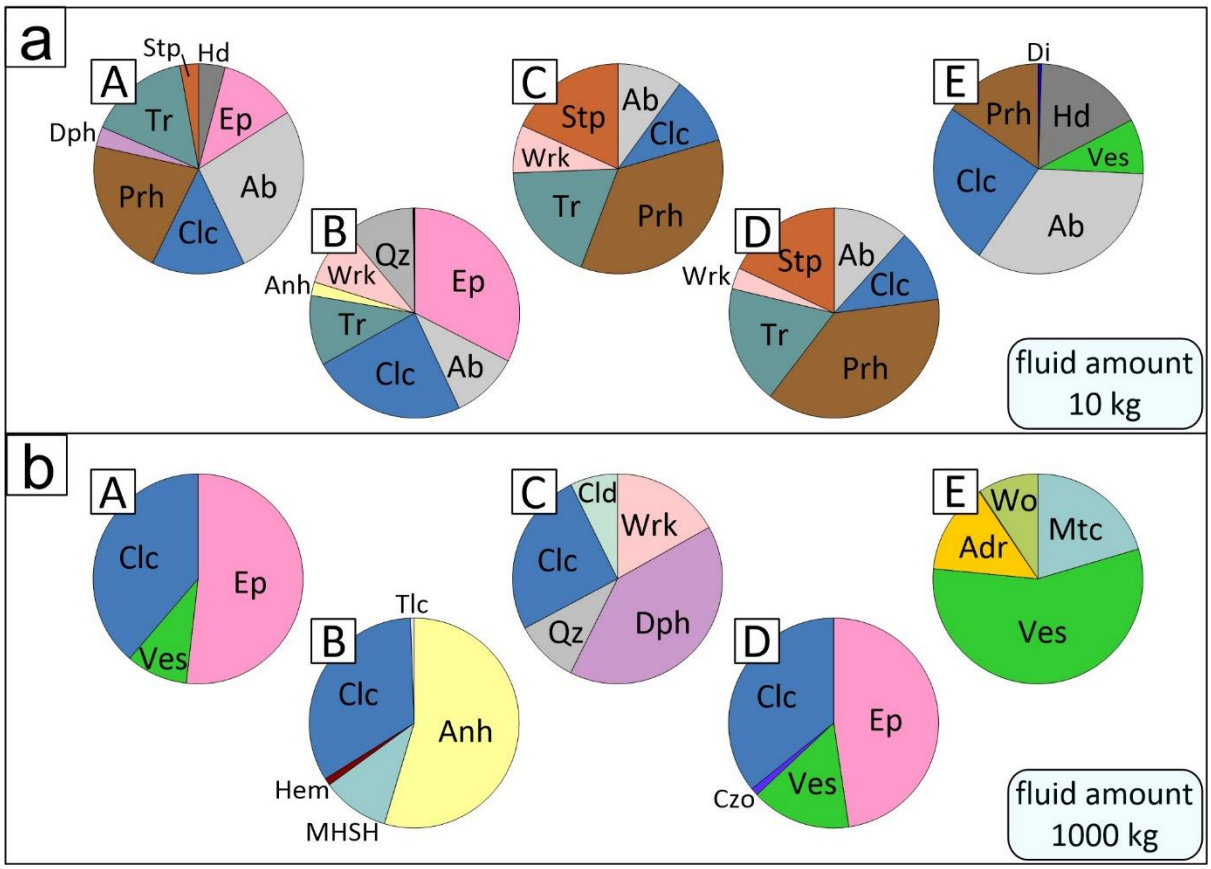


*Figure 2 Modal composition predicted from alteration of gabbro (1 kg) at 300°C depending on fluid amount and fluid composition: a) low fluid amount (10 kg) b) high fluid amount (1000 kg). Capital letters denote different fluid compositions as presented in Table 1. Modal proportions of minerals were calculated from molal amounts based on average density for each mineral published at [www.webmineral.com](http://www.webmineral.com) (densities are available in Table SX). Ab: albite, Adr: andradite, Anh: anhydrite, Clc: clinochlore, Cld: chloritoid, Czo: clinozoisite, Di: diopside, Dph: daphnite, Ep: epidote, Hd: hedenbergite, Hem: hematite, MHSH: magnesium-hydroxide-sulphate-hydrate, Mtc: monticellite, Prh: prehnite, Qz: quartz, Stp: stilpnomelane, Tlc: talc, Tr: tremolite, Ves: vesuvianite, Wo: wollastonite, Wrk: wairakite.*

## 3.2 A closer look on the model *E* (Seyfried's solution)

Model *E*, which uses the experimental serpentinization fluid composition from Seyfried et al. (2007), predicts the highest content of the mineral phase of interest, i.e. vesuvianite, as shown in the previous section. Figure 3 shows the evolution of mineralogy as a function of the fluid amount over the whole range 10 – 1000 kg. Phases predicted at low fluid amount (hedenbergite, prehnite) disappear gradually with increasing fluid amount and are missing in the system above 50 kg of fluid. Similarly, the amount of albite decreases and reaches zero at fluid amount around 300 kg. At a medium fluid amount (50 – 500 kg), the assemblage is characterized by presence of Na, K-bearing phases such as phlogopite and annite. The content of diopside increases progressively and is only replaced by wollastonite and monticellite at high fluid amount around 700 kg. Interestingly, clinochlore is predicted at a low fluid amount (< 100 kg) and a high fluid amount (> 500 kg) but it is lacking in the medium interval. Andradite is present in the system at fluid amount above 300 kg. The content of vesuvianite increases progressively with increasing fluid amount. Overall, mineralogy evolves from a typical prehnite-pumpellyite facies assemblage (prehnite, albite, chlorite) at a low fluid amount (< 300 kg) to a rodingitic assemblage (andradite, vesuvianite, diopside) for a higher fluid amount (> 300 kg).

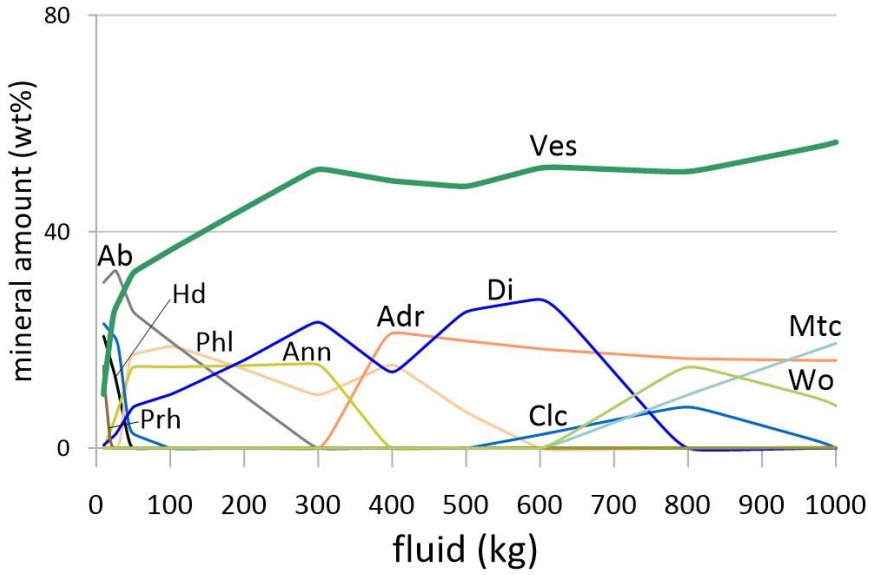


*Figure 3 Calculated mineral composition depending on fluid amount from the reaction of gabbro with the Seyfried's solution (model E) at 300°C. Ab: albite, Adr: andradite, Ann: annite, Clc: clinochlore, Di: diopside, Hd: hedenbergite, Mtc: monticellite, Phl: Na-phlogopite, Prh: prehnite, Ves: vesuvianite, Wo: wollastonite.*

Changes in the whole rock chemistry of the altered rock have been quantified and are presented in figure 4. The amount of mobile elements such as Na and K mirrors the presence of phlogopite and annite in the predicted mineralogy (Fig. 3), i.e. these elements are progressively leached out completely from the solid phase as micas are dissolved in the fluid. Si and Al amounts decrease at a medium fluid amount (300 – 500 kg) to 83 and 70 %, respectively, of their initial content. This is explained by the disappearance of albite and the appearance of diopside (Fig 3). At a high fluid amount (800 – 1000 kg), interestingly, the absolute amount of Si and Al increase again and reach up to values approaching their initial amounts (103 and 92 %, respectively) as large amounts of wollastonite and monticellite precipitates. The amounts of Mg and Fe remain unchanged in the system (Fig 4). It is important to note, however, that none of these elements is present in the initial fluid, therefore, no enrichment is possible considering these elements. The most interesting feature of the chemical evolution is the continuous enrichment in Ca, which reaches progressively up to 400 % at a very high fluid amount (1000 kg). Ca enrichment is reflected by the precipitation of diopside, andradite, monticellite and wollastonite. This significant Ca fixation also dominantly contributes to an overall increase in total mass of the modeled rock, from 1000 to 1369 grams (Fig. 4). It is interesting to note that the calculated whole rock compositions (Table 2, Fig. 5) show a significant and progressive decrease in $SiO_2$ content (51.97 down to 38.77 wt.%) while the CaO content increases from 12.84 up to 37.32 %. As a result of Ca fixation (Fig. 4), the relative contents of other components ($Al_2O_3$, FeO, MgO, $Na_2O$, $H_2O$) are generally decreasing with increasing amount of fluid in the system (Table 2, Fig. 5).

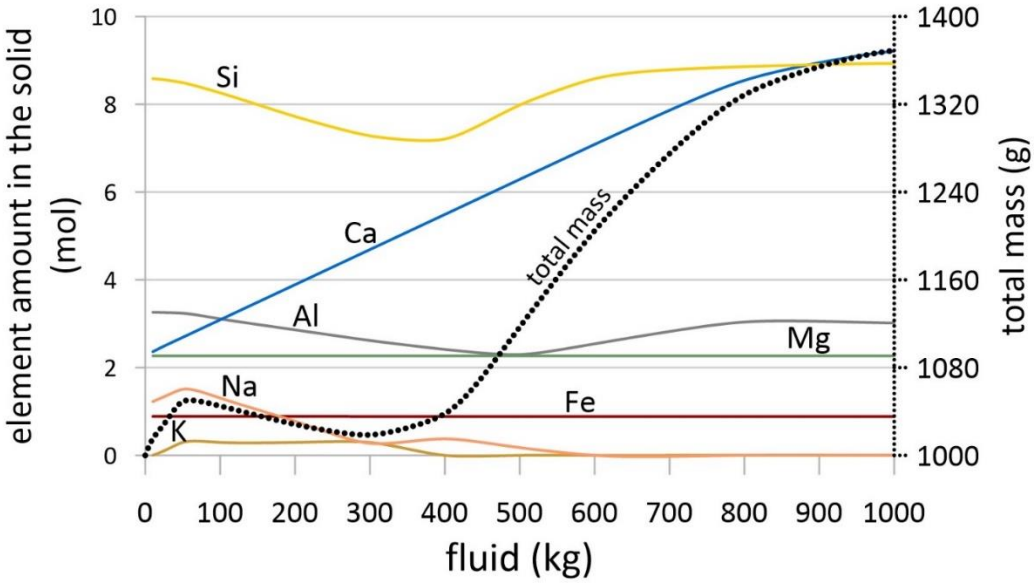


*Figure 4 Element amounts in the modeled solid phase depending on fluid amount from the reaction of 1 kg of gabbro with the Seyfried's solution (model E) at 300°C. Values were manually quantified from mineral amounts (and their respective compositions) calculated in the model. Note the progressive and significant Ca-enrichment with increasing fluid amount in the system. Ca-enrichment is also responsible for the increase of total mass of the solid phase.*

*Table 2 Recalculated whole rock composition (in wt.%, normalized on 100 %) of the altered rock resulting from the interaction of 1 kg of gabbro with variable amount of the Seyfried's solution (model E) at 300°C. Values were manually quantified from mineral amounts (and their respective compositions) calculated in the model. These values are shown in a graphical form in figure 5.*

| fluid amount | 0 kg | 10 kg | 100 kg | 500 kg | 1000 kg |
|---|---|---|---|---|---|
| $SiO_2$ | 51.97 | 49.18 | 47.09 | 42.41 | 38.77 |
| $Al_2O_3$ | 16.58 | 15.85 | 15.04 | 10.35 | 11.10 |
| FeO | 6.38 | 6.08 | 6.05 | 5.63 | 4.60 |
| CaO | 12.84 | 12.62 | 16.44 | 31.19 | 37.32 |
| MgO | 9.14 | 8.72 | 8.67 | 8.08 | 6.60 |
| $Na_2O$ | 3.03 | 3.62 | 3.85 | 0.52 | 0.00 |
| $K_2O$ | 0.06 | 0.00 | 0.00 | 0.00 | 0.00 |
| $H_2O$ | 0.00 | 3.93 | 2.85 | 1.83 | 1.61 |

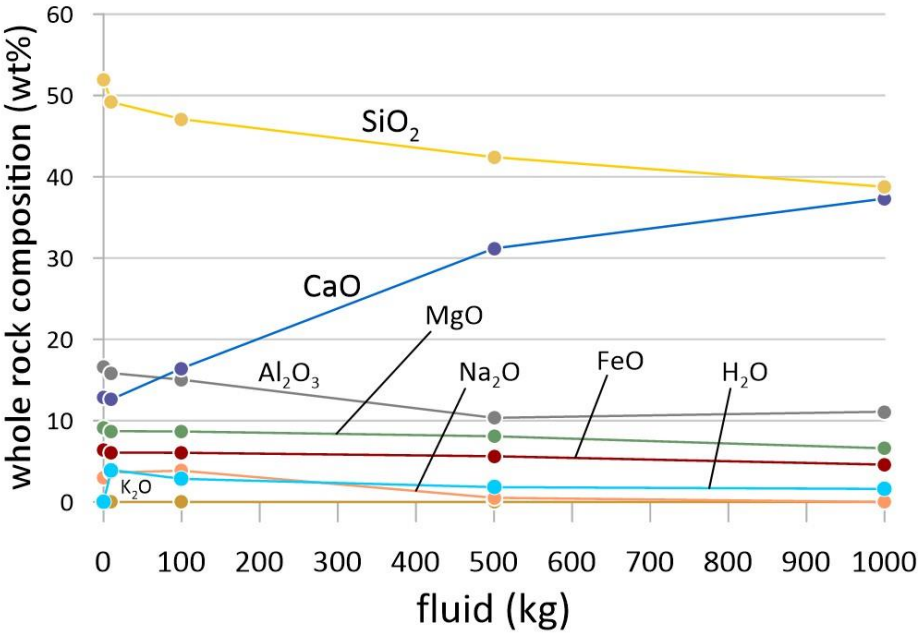


*Figure 5 Graphical representation of the recalculated whole rock composition (Table 2) of the altered rock resulting from the interaction of 1 kg of gabbro with variable amount of the Seyfried's solution (model E) at 300°C. Note the decreasing $SiO_2$ and increasing CaO demonstrating the most typical changes in whole-rock chemistry during the rodingitization.*

## 3.3 Sensitivity test to fluid compositions

### 3.3.1 Principles of the sensitivity test

In section 3.1, we have shown that both experimental serpentinization fluids (Klein's solution used in model *D* and Seyfried's solution used in model *E*) lead to the stabilization of significant vesuvianite in the modeled rock if the amount of fluid in the system is sufficiently high. Consequently, we select these two fluids as initial solutions for investigation of the influence of changes in fluid composition on predicted mineral assemblages. It remains challenging to explore all fluid composition changes because the fluid chemistry is defined by numerous variables and it is not possible to vary and explore all variables at the same time. This is why *one-factor-at-a-time* method is applied on each experimental fluid to quantify the effect of each variable separately. This means that at every calculation, all but one variable are constant and the influence of this variable is investigated in detail. Following variables are tested: Ca, Mg, Si, Al, Na, K, C, S, $H_2$, reduction-oxidation potential (pe) and pH. The fluid amount is invariably set to 1000 kg.

### 3.3.2 Sensitivity test # 1 (Klein's solution)

The influence of Ca concentration in the initial fluid on the calculated mineral assemblage is presented in Figure 6a. The diagram shows that at very low Ca concentration (< 2 mmol/kg), albite and daphnite are present in the system. However, at higher Ca concentration, the amounts of predicted phases represented by epidote, clinochlore, clinozoisite and vesuvianite remain constant.

The increase of Mg concentration causes the disappearance of vesuvianite from the system as soon as the Mg concentration reaches 1 mmol/kg, and decrease and disappearance of epidote at around 2 mmol/kg (Fig. 6b). Clinozoisite and daphnite occur in the secondary assemblage when the Mg concentration is around 2 mmol/kg but they disappear progressively at higher concentration. The amount of clinochlore increases with increasing Mg concentration. At higher Mg concentration, phyllosilicates (clinochlore, amesite) are the only predicted phases in the resulting rock.

At very low Si concentration, the predicted assemblage consists of epidote and clinochlore (Fig. 6c). Diopside appears at 1 mmol/kg and is abundant in the assemblage above this value. Prehnite is present only in a limited range of Si concentration (4 – 16 mmol/kg). Hedenbergite appears at 8 mmol/kg while quartz and wollastonite are present in the system if the Si concentration is above 12 mmol/kg. The amount of vesuvianite increases slightly with increasing Si concentration and coexistence of vesuvianite and quartz is predicted in this case.

In a wide range of pH values (4 – 10), the mineral assemblage consisting of epidote, clinochlore and vesuvianite remains the same (Fig. 6d). However, significant changes in mineralogy occur above pH 10. Epidote and clinochlore disappear while andradite, a common rodingite mineral, appears in the assemblage. Most importantly, the amount of vesuvianite increases significantly at high pH values. At a very extreme pH (> 12), monticellite, wollastonite, brucite and rankinite appear in the system.

Changes in other investigated variables in the fluid composition have only marginal or any effect on the predicted mineral assemblage. These results can be found in supplementary material (Table SX).

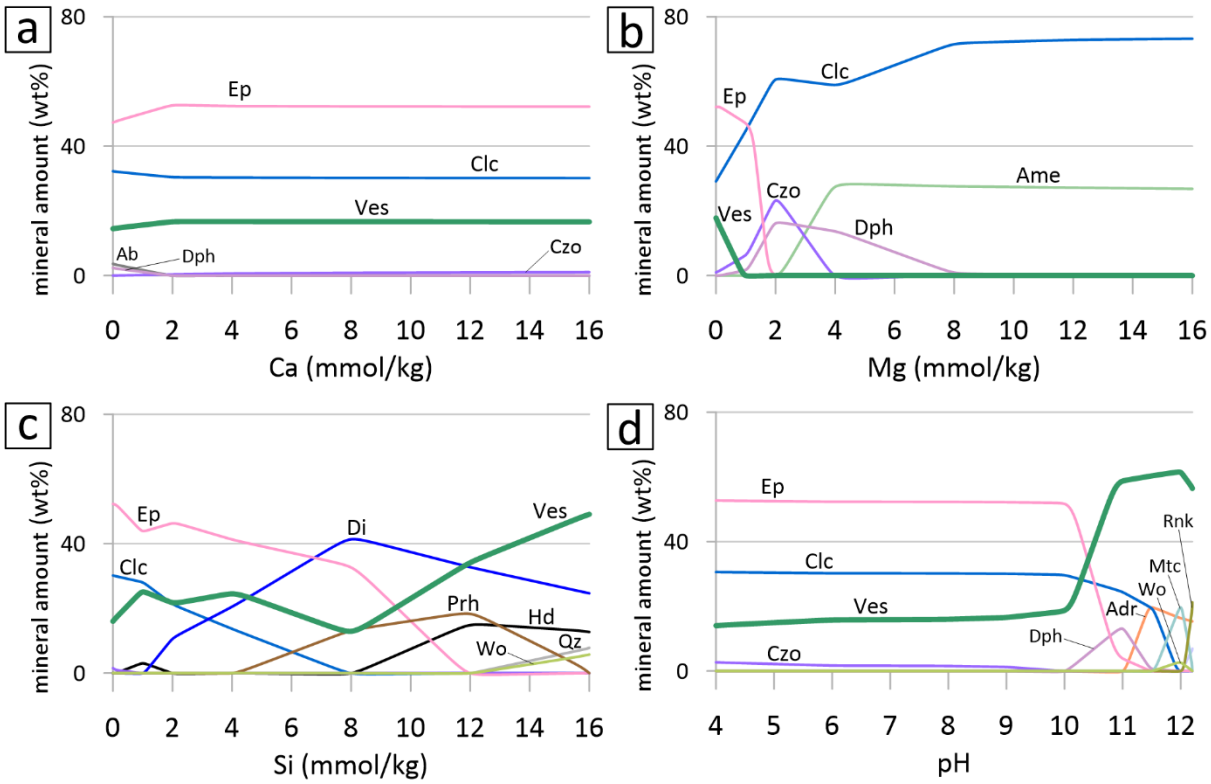


*Figure 6 Influence of changes in fluid composition on the predicted mineralogy explored by one-factor-at-a-time method applied on experimental serpentinization fluid from Klein et al. (2015) (model D), 300°C, fluid amount 1000 kg. a) variable Ca concentration. b) variable Mg concentration. c) variable Si concentration. d) variable initial pH. Ab: albite, Adr: andradite, Ame: amesite, Br: brucite, Clc: clinochlore, Czo: clinozoisite, Di: diopside, Dph: daphnite, Ep: epidote, Hd: hedenbergite, Mtc: monticellite, Prh: prehnite, Qz: quartz, Rnk: rankinite, Ves: vesuvianite, Wo: wollastonite.*

### 3.3.3 Sensitivity test # 2 (Seyfried's solution)

If the Ca concentration in the fluid is low (< 2 mmol/kg), the predicted assemblage consists of diopside, Na-phlogopite, andradite and vesuvianite (Fig. 7a). The amount of vesuvianite increases at low concentration (< 8 mmol/kg) and then remains stable above this value. Andradite is the only Fe-bearing phase in the system and its amount is thus not affected by changes in Ca concentration. At Ca

concentration between 4 – 10 mmol/kg, phases such as monticellite, clinochlore and wollastonite appear in the system. Brucite and rankinite are present above 8 mmol/kg. At high Ca concentration (> 12 mmol/kg), the assemblage consists of andradite, vesuvianite, larnite, brucite and rankinite.

A small increase in Mg concentration in the fluid (from 0 to 2 mmol/kg) causes a significant increase of the amount of brucite and disappearance of wollastonite (Fig. 7b). Vesuvianite and monticellite are present at lower Mg concentration (< 16 mmol/kg) but disappear completely at values around 24 mmol/kg. At higher Mg concentration (> 20 mmol/kg), the predicted assemblage consists of clinochlore, diopside, andradite and a serpentine phase (antigorite). Andradite is replaced by troilite when the Mg concentration exceeds 24 mmol/kg.

At low Si concentration (< 3 mmol/kg), the assemblage consists of vesuvianite, wollastonite, monticellite, andradite and clinochlore. Increasing Si concentration decreases the amount of vesuvianite until its complete disappearance at around 16 mmol/kg (Fig. 7c). Diopside and albite appear at 3 mmol/kg and 8 mmol/kg, respectively, and their amounts increase progressively with increasing Si concentration. The amount of andradite remains stable in a wide range of Si concentration and is only replaced by hedenbergite when the Si concentration exceeds 24 mmol/kg. At very high Si concentration (> 24 mmol/kg), the predicted assemblage consists of wollastonite, albite and pyroxenes (diopside and hedenbergite).

In a wide range of pH values (4 – 10.5), the mineral assemblage consisting of diopside, vesuvianite and troilite remains virtually the same (Fig. 7d). Similarly to the first sensitivity test (section 3.3.1), significant changes in the predicted mineralogy occur at higher pH values (> 10.5). Most notably, andradite replaces troilite and diopside is replaced by monticellite and wollastonite at very high pH (> 11.5). Clinochlore also appears at pH above 11. In this case, the amount of vesuvianite remains almost without changes even at high pH.

As in the first sensitivity test, we note that Ca, Mg, Si content and pH have the most significant influence on the predicted mineral assemblage. Changes in other investigated variables in the fluid composition (see supplementary material (Table SX)) have only marginal effect.

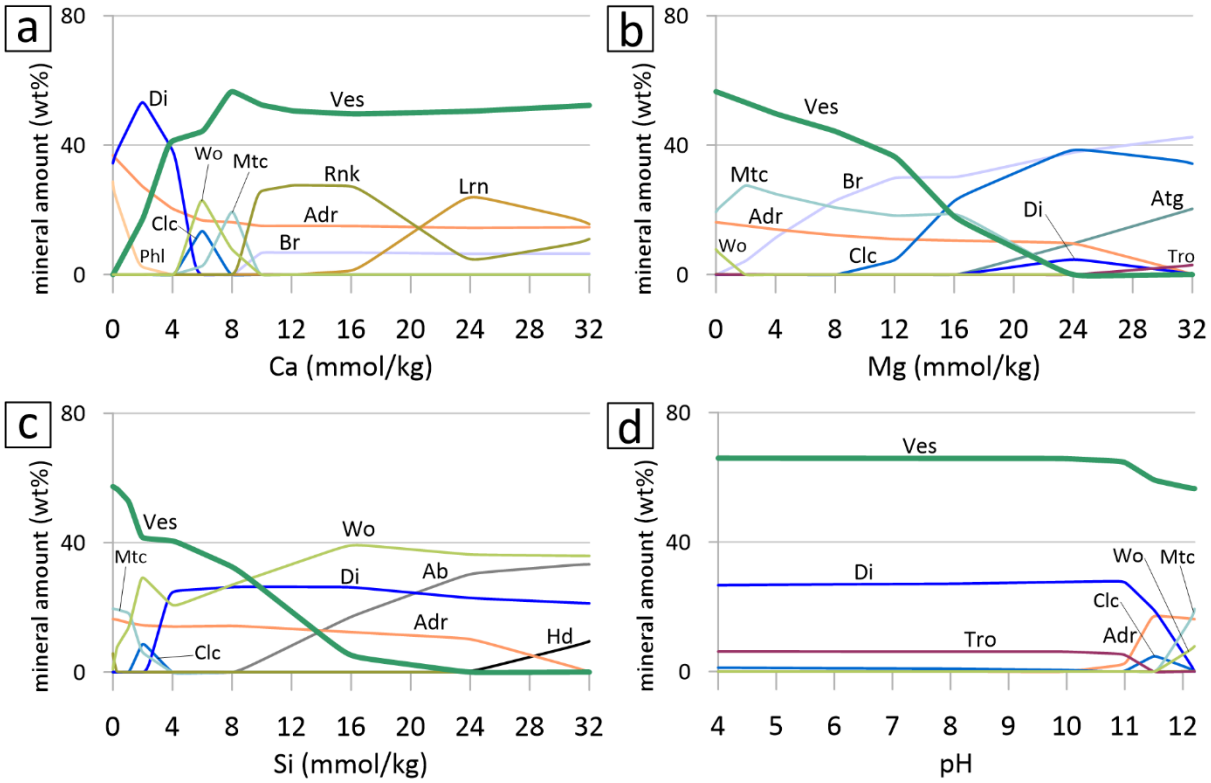


*Figure 7 Influence of changes in fluid composition on the predicted mineralogy explored by one-factor-at-a-time method applied on experimental serpentinization fluid from Seyfried et al. (2007) (model E), 300°C, fluid amount 1000 kg. a) variable Ca concentration. b) variable Mg concentration. d) variable initial pH. Ab: albite, Adr: andradite, Atg: antigorite, Br: brucite, Clc: clinochlore, Di: diopside, Hd: hedenbergite, Lrn: larnite, Mtc: monticellite, Phl: Na-phlogopite, Rnk: rankinite, Tro: troilite, Ves: vesuvianite, Wo: wollastonite.*

# 4 Discussion

## 4.1 Progress of the rodingitization process

Ca enrichment and Si leaching are chemical changes occurring during the rodingitization process that are well outlined by our calculations (Table 2, Fig. 5). They represent the most notable changes in whole rock composition and as such are commonly used to express the extent of the rodingitization process (Koutsovitis et al., 2013; Laborda-López et al., 2020; Rogkala et al., 2022; Duan et al., 2022; Butek et al., 2022). Consequently, we suggest that a single variable, the molal ratio Si/Ca, can serve as a proxy to determine the extent of transformation. A review of literature data (Fig. 8) shows that fresh gabbroic rocks normally display a Si/Ca value between 3.4 – 4.4 (MacLeod et al., 2017). This ratio decreases significantly during rodingitization and the majority of vesuvianite-bearing rodingites from the literature display a Si/Ca value between 1 – 2 (Li et al., 2004, 2007, 2017; Kobayashi and Kaneda, 2010; Koutsovitis et al., 2013; Fukuyama et al., 2014; Dai et al., 2016; Salvioli-Mariani et al., 2020; Mubarak et al., 2020; Rogkala et al., 2022; Butek et al., 2022). The evolution of the Si/Ca value as a function of the fluid amount for model *E* is reported in Figure 8 and shows continuous, albeit non-linear, decrease in the Si/Ca value with increasing amount of fluid. The shift quantified from our calculations (from 3.75 to 1) is in good agreement with the shift observed during the transformation of natural gabbros into rodingites. Most importantly, geochemical model *E* confirms that a significant extent of rodingitization (as indicated by fluid amount above 200 kg) is required for the formation of vesuvianite-bearing rodingites (Fig. 8).

Our calculations consistently show that increasing fluid amount results in an increasing quantity of vesuvianite (Figs. 2 and 3). This finding is also in good agreement with the thermodynamic model presented by Palandri and Reed (2004), where the interaction of a pyroxene-rich gabbro with a serpentinization fluid predicts vesuvianite only at a water-rock ratio above 200. Such high water-rock ratio can be hard to imagine considering the constraints from O isotopes studies suggesting a relatively low fluid-rock ratio (< 10) during serpentinization (Rouméjon et al., 2015; Zhao et al., 2023). However, these studies often focus on only partially serpentinized ultramafic rocks very probably forming at the beginning of the alteration (at lower fluid-rock ratio). Rodingites occur almost exclusively in completely serpentinized rocks (Katoh and Niida, 1983), which suggests a higher fluid amount participating in the process (Rouméjon et al., 2015, 2018). A high fluid amount can be achieved in nature either by a small to moderate fluid influx continuing for a long time, or by a very high fluid volume in contact with the rock during a short time. We assume the former option more plausible since it allows to advance the mineral reactions to the chemical equilibrium more easily. In any case, we conclude that vesuvianite formation requires an open system with a significant input of a fresh hydrothermal fluid.

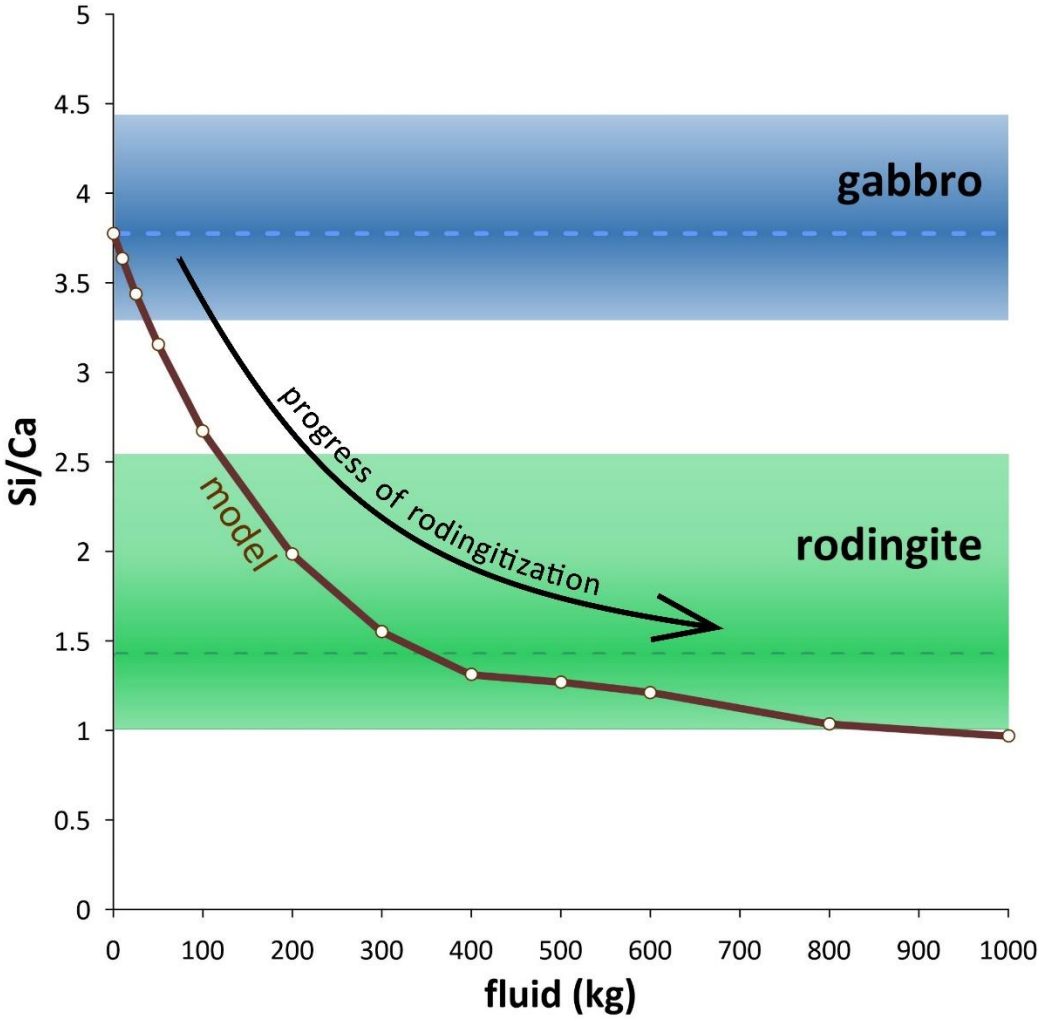


*Figure 8 Diagram of Si/Ca (molal ratio) in the solid phase vs fluid amount in the system. It compares the calculated chemical composition (brown line, model E, section 3.2) with natural samples. Blue area represents gabbro compositions (n = 201) from a present seafloor, oxide-rich samples excluded (MacLeod et al., 2017). Green area represents vesuvianite-bearing rodingite compositions (n = 49) from the literature (Li et al., 2004, 2007, 2017; Kobayashi and Kaneda, 2010; Koutsovitis et al., 2013; Fukuyama et al., 2014; Dai et al., 2016; Salvioli-Mariani et*

*al., 2020; Mubarak et al., 2020; Rogkala et al., 2022; Butek et al., 2022). Top and bottom 5% of data were excluded from both datasets to remove outliers. Dashed horizontal lines represent the average composition in each dataset. The progressive transition from gabbroic composition to rodingite (rodingitization) is characterized by decreasing Si-Ca ratio.*

## 4.2 Volume changes during the rodingitization process

Rodingitization is often assumed to be a constant volume process in the published literature. This assumption is mostly based on mass balance calculations (Schandl et al., 1989; Normand, 2001; Puschnig, 2002), but it is also supported by the absence of signs of deformation induced by volume changes observed in the field (Nishiyama et al., 2017). However, model *E* in this contribution predicts a significant increase in the total mass of the rock (from 1000 to 1369 g at 1000 kg of fluid), primarily caused by the fixation of Ca (Fig. 4). An average gabbro has a density of around 3 g/cm$^3$ and the calculated density of the modeled rodingite is 3.38 g/cm$^3$, indicating a clear increase in rock density during rodingitization. Despite this, if we translate the mass change into a change in volume, it still results in about a 20 % increase in volume. We propose three explanations for the fact that volume increase during rodingitization is not reported in the literature: 1) extremely rodingitized rocks presented by high amounts of fluid in this study are quite rare in nature; 2) rodingitized rocks can increase their volume, but this fact is hardly observed in the field because the plasticity of surrounding serpentinite can eventually absorb the increase in volume; and 3) the variation in mineral composition influences rock density. Since garnet is the densest mineral among the rodingite paragenesis, it could be that rodingite samples very rich in garnet will not undergo significant volume changes. On the other hand, however, rodingites relatively poor in garnet would still undergo a volume increase as predicted by our calculations.

## 4.3 Modeled mineralogy vs. natural rodingites

Natural mafic rocks affected only by a low extent of hydrothermal alteration commonly contain relics of primary minerals and the hydrothermal (secondary) paragenesis consists of prehnite, chlorite, epidote-clinozoisite, albite or tremolite (Schandl et al., 1989; Attoh et al., 2006; Li et al., 2017; Wang et al., 2019; Duan et al., 2021, 2022). These phases are consistently predicted in our calculations at low fluid amounts (Figs. 2 and 3), indicating their precipitation during the early stages of the rodingitization process.

Chlorite-group minerals are widespread in hydrothermal rocks in general and are present in virtually all natural rodingites, whether affected by a low or high degree of alteration. Accordingly, these minerals are commonly predicted in our models. Since diopside and garnet represent the most abundant phases in the majority of rodingites described in the literature, they can be presumably considered the most important transition phases between slightly rodingitized and extensively rodingitized rocks (Schandl et al., 1989; Li et al., 2017), and together with vesuvianite, they are probably the best indicators of a typical rodingite paragenesis (Fig. 6d, 7d). Some of the minerals predicted in our models are rare or have never been described in natural rodingites. Such phases are represented by wollastonite, rankinite, monticellite or troilite. We assume that these discrepancies are mainly due to the limitations of the thermodynamic dataset and the absence of solid solutions.

Natural gabbroic rocks affected by a significant extent of rodingitization are generally characterized by the presence of more or less abundant vesuvianite (Li et al., 2004, 2007, 2008, 2017; Zanoni et al., 2016; Duan et al., 2022; Butek et al., 2022). In vesuvianite-dominated samples of extensively rodingitized rocks from the Zermatt-Saas ophiolite (Li et al., 2008; Zanoni et al., 2016) and the Western Carpathians (Butek et al., 2022), the characteristic mineralogy comprises vesuvianite, diopside, garnet (grossular – andradite series) and clinochlore in variable proportions. This assemblage is very well retrieved in a model characterized by a high amount of experimental serpentinization fluid at 300°C,

with pH modified to 11.5 (Fig. 7d), which predicts a modal proportion of Ves = 59.8 %, Clc = 21.1 %, Di = 11.8 %, Adr = 7.3 % (Fig. 9).

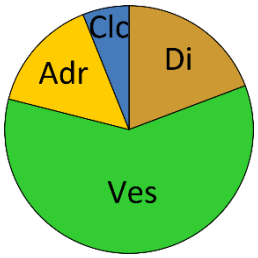


*Figure 9 Calculated modal composition of the altered rock resulting from the interaction of 1 kg of gabbro with 1000 kg of the Seyfried's solution (model E) modified to pH 11.5, at 300°C. Vesuvianite constitutes more than 50 % of the sample and the mineral assemblage is in very good agreement with majority of extensively rodingitized rocks described in the literature. Adr: andradite, Di: diopside, Clc: clinochlore, Ves: vesuvianite.*

## 4.4 Composition of the rodingitization fluid

Experimental studies investigating the chemical exchanges between seawater and basalt have shown that Ca is commonly leached from the mafic rock during hydrothermal alteration (Seyfried and Bischoff, 1981; Mottl, 1983; Alt, 1995). While this is true for fluids of seawater composition or evolved fluids with low pH (< 8), it seems that fluids equilibrated with serpentinite, characterized by high pH (> 10; Barnes et al., 1978; Kelley et al., 2001), induce the opposite: Ca fixation. In this case, Ca is removed from the fluid and incorporated into the altered rock (cf. Seyfried et al., 1998). This is in good agreement with the progressive Ca enrichment in the solid phase predicted by our model (Fig. 4), and it is also confirmed by numerous mass balance calculations for natural protolith-rodingite pairs (Koutsovitis et al., 2013; Tsikouras et al., 2013; Li et al., 2017; Rogkala et al., 2022; Karkalis et al., 2022).

Since the rodingitization process unquestionably includes Ca enrichment in the protolith, it is commonly termed as *Ca metasomatism*. This leads to the prevailing assumption that a Ca-rich hydrothermal fluid with high Ca activity is involved in the hydrothermal process (e.g. Puschnig, 2002; Hatzipanagiotou et al., 2003; Li et al., 2004). Despite the fact that Ca enrichment is significant in most rodingites, several authors have already doubted this idea in the past and suggested that low $SiO_2$ activity and silica leaching are the key factors driving rodingite formation (Normand, 2001; Frost et al., 2008; Bach and Klein, 2009). Our calculations show that vesuvianite can be stabilized during fluid-rock interaction involving pure water, i.e. even if no Ca is available in the fluid (Fig. 2b). Furthermore, the sensitivity tests (Figs 6a, 7a) show that a change in Ca concentration of the fluid does not significantly affect neither the predicted amount of vesuvianite nor the amount of andradite. Consequently, we agree with the idea that rodingitization is not induced by high Ca activity and that high Ca concentration (> 10 mmol/kg) in the circulating hydrothermal fluid is not required for the process to occur.

On the other hand, our models show that the hydrothermal fluid must be low in magnesium to trigger the formation of vesuvianite (Fig. 6b, 7b). In other words, the high MgO content of serpentinized ultramafic rocks, as the prime host of rodingites, could eventually inhibit the formation of vesuvianite-bearing rodingite. However, experimental studies simulating serpentinization (e.g. Seyfried et al., 2007) show that Mg is not only retained in the serpentinized rock during the process, but it is even transferred from the fluid into the serpentinite. This fact is also confirmed by measured compositions of natural serpentinization fluids displaying very low Mg concentrations (Barnes et al., 1978; Kelley et

al., 2001). The serpentinization process thus effectively buffers the Mg concentration in the fluid near zero, which is presumably essential for the rodingitization process to occur. Rodingites are commonly lighter in Mg isotopic composition than their protolit (Dai et al., 2016; Zhao et al., 2023; Xiong et al., 2024). This fact does not support well the idea of a low-Mg fluid because some Mg (0.45 - 0.99 wt% MgO; Zhao et al., 2023) must be dissolved in the fluid to cause the Mg low isotopic signature. It seems probable that a water-ratio higher than 10 (cf. Xiong et al., 2024), and another process(es) should be considered to adequatly explain the Mg isotopic fractionation during fluid-gabbro interactions. More research is needed to clarify this inconsistency. Li et al. (2017) calculated that a high CaO/MgO activity [μ(CaO/MgO)] is required to form vesuvianite-bearing rodingite. According to our results (Figs. 6b, 7b) and the fact that Ca concentration does not have much effect on the predicted amount of vesuvianite, we assume that the higher μ(CaO/MgO) value in the Si vs Ca/Mg activity diagram presented by Li et al. (2017) is mostly controlled by a decrease in MgO, and not much by an increase in CaO.

Similarly to Mg, the Si content in the fluid should be low to trigger the formation of vesuvianite-bearing rodingites (Fig. 7c). This is consistent with the progressive desilication during rodingitization as discussed above (section 4.1), even though desilication was calculated in our model to occur only at lower fluid amounts (below 400 kg) (Fig. 4). Hydrothermal vent fluid compositions (Fouquet et al., 2010; Seyfried et al., 2015) as well as experimental studies (Wetzel and Shock, 2000) show a systematic difference in Si concentration between the hydrothermal fluid from an ultramafic (peridotite-dominated) system and the fluid from a mafic (basalt-gabbro) system. Low-Si hydrothermal fluid is characteristic of ultramafic systems, while higher Si concentrations in the fluid indicate an interaction with a mafic rock, which can result in the precipitation of quartz during alteration (Mottl, 1983; Fletcher et al., 1997; Wetzel and Shock, 2000). Based on this fact, we suggest that a large volume of ultramafic rock undergoing serpentinization compared to smaller mafic bodies undergoing rodingitization leads to low Si activity in the whole system and induces silica leaching from the mafic lithology.

Predicted mineral assemblages are significantly affected by the initial pH of the hydrothermal fluid. The reaction with evolved seawater (model *D*) yields rodingite minerals only at a very high pH (11 – 12; Fig. 6d) and the amount of vesuvianite increases with increasing pH. Therefore, we suggest that a high pH of the hydrothermal fluid favours the formation of vesuvianite-bearing rodingites. Since serpentinization fluids are commonly characterized by high pH values (Barnes et al., 1978; Kelley et al., 2001), this result is consistent with the general concept that the rodingitization process is driven by the presence of an alkaline serpentinization–related fluid and that the serpentinization and rodingitization processes are both spatially and temporally connected (Palandri and Reed, 2004).

Rodingite forming fluid is typically considered to be very low in $CO_2$ ($X_{CO2} < 10^{-4}$). This knowledge originates from numerous thermodynamic calculations indicating vesuvianite instability at higher $CO_2$ concentrations (Rice, 1983; Li et al., 2008; Duan et al., 2021), but also from several fluid inclusion studies that do not report significant $CO_2$ concentration in the hydrothermal fluid (Schandl et al., 1990; O'Hanley et al., 1992; Murzin and Shanina, 2007; Normand and Williams-Jones, 2007). However, our sensitivity tests on fluid composition suggest that vesuvianite formation is not necessarily inhibited at significant $CO_2$ (Table SX) and thus even the coexistence of vesuvianite and calcite could be eventually possible, as has been already observed in some natural rodingites (Salvioli-Mariani et al., 2020; Butek et al., 2022). We agree with Salvioli-Mariani et al. (2020) who drew the same conclusion from their thermodynamic calculations, namely that low $CO_2$ concentration are not required for the rodingitization process.

# 5 Conclusion

- An open system with a high amount of hydrothermal fluid is required to transform a mafic protolith into rodingite. The most rodingitized rocks are characterized by the presence of vesuvianite, which is stabilized only at a very high fluid-rock ratio.
- The evolution of the whole rock composition (namely Ca enrichment and Si leaching) during rodingitization is successfully simulated by our calculations. Consequently, the progress of rodingitization can be quantified by the Si/Ca value in the rock because this ratio progressively decreases during the continuous metasomatic transformation.
- Geochemical modeling of gabbro-fluid interactions at 300°C adequately reproduces rodingite parageneses in a large range of fluid compositions. Moreover, it shows that the significant heterogeneity in the mineralogy of natural rodingite samples is induced mainly by variation in the amount of fluid affecting the hydrothermal system.
- A Ca-rich fluid is not required to induce rodingitization. However, the fluid must be devoid of Mg and low in Si. This composition can be derived from evolved seawater and is naturally controlled by the serpentinization process simultaneously occurring in the surrounding rocks.
- High pH and reducing conditions generally favour vesuvianite precipitation and are presumably favourable to the formation of rodingite paragenesis. This is consistent with the composition of serpentinization fluids and underlines the fact that the process of rodingitization is driven by a serpentinization fluid.


## Acknowledgements

We thank Yi-Xiang Chen and one anonymous reviewer for their constructive comments which substantially improved the final version of the manuscript. This research was funded by the TelluS Program of CNRS/INSU and the Slovak Research and Development Agency (APVV-22-0092). The international cooperation was supported by the PHC Stefanik program and the bilateral project SK-FR-22-0010.

# 6 References


Aksenov, S.M., Chukanov, N.V., Rusakov, V.S., Panikorovskii, T.L., Rastsvetaeva, R.K., Gainov, R.R., Vagizov, F.G., Lyssenko, K.A., and Belakovskiy, D.I., 2016, Towards a revisitation of vesuvianite-group nomenclature: the crystal structure of Ti-rich vesuvianite from Alchuri, Shigar Valley: Acta Crystallographica Section B Structural Science, Crystal Engineering and Materials, v. 72, p. 744–752, doi:10.1107/S2052520616010246.

Alt, J.C., 1995, Subseafloor Processes in Mid-Ocean Ridge Hydrothermal Systems, *in* Humphris, S.E., Zierenberg, R.A., Mullineaux, L.S., and Thomson, R.E. eds., Seafloor Hydrothermal Systems, Washington, D. C., American Geophysical Union, Geophysical Monograph Series 91, p. 85–114, doi:10.1029/GM091p0085.

Anderson, G.M., 2005, Thermodynamics of natural systems: Cambridge University Press.

Appelo, C.A.J., Parkhurst, D.L., and Post, V.E.A., 2014, Equations for calculating hydrogeochemical reactions of minerals and gases such as CO2 at high pressures and temperatures: Geochimica et Cosmochimica Acta, v. 125, p. 49–67, doi:10.1016/j.gca.2013.10.003.

Attoh, K., Evans, M.J., and Bickford, M.E., 2006, Geochemistry of an ultramafic-rodingite rock association in the Paleoproterozoic Dixcove greenstone belt, southwestern Ghana: Journal of African Earth Sciences, v. 45, p. 333–346, doi:10.1016/j.jafrearsci.2006.03.010.

Bach, W., Jöns, N., and Klein, F., 2013, Metasomatism Within the Ocean Crust, *in* Metasomatism and the Chemical Transformation of Rock, Berlin, Heidelberg, Springer Berlin Heidelberg, Lecture Notes in Earth System Sciences, p. 253–288, doi:10.1007/978-3-642-28394-9_8.

Bach, W., and Klein, F., 2009, The petrology of seafloor rodingites: Insights from geochemical reaction path modeling: Lithos, v. 112, p. 103–117, doi:10.1016/j.lithos.2008.10.022.

Barnes, I., O'Neil, J.R., and Trescases, J.J., 1978, Present day serpentinization in New Caledonia, Oman and Yugoslavia: Geochimica et Cosmochimica Acta, v. 42, p. 144–145, doi:10.1016/0016-7037(78)90225-9.

Butek, J., Dufourcau, D., Duchene, S., Laurent, O., Grégoire, M., and Spišiak, J., 2023, A petrochronological study of FeTi oxides in rodingites of the Western Carpathians, Slovakia: Lithos, v. 460–461, p. 107393, doi:10.1016/j.lithos.2023.107393.

Butek, J., Grégoire, M., Spišiak, J., Duchene, S., and Kopáčik, R., 2022, On the origin of vesuvianite-rich rodingites from the Western Carpathians, Slovakia: Lithos, v. 432–433, p. 106902, doi:10.1016/j.lithos.2022.106902.

Charlou, J.L., Donval, J.P., Fouquet, Y., Jean-Baptiste, P., and Holm, N., 2002, Geochemistry of high H2 and CH4 vent fluids issuing from ultramafic rocks at the Rainbow hydrothermal field (36j14VN, MAR): Chemical Geology, p. 15.

Coleman, R.G., 1967, Low-temperature reaction zones and alpine ultramafic rocks of California, Oregon, and Washington: Geological Survey Bulletin, doi:10.3133/b1247.

Dai, J.G., Wang, C.S., Liu, S.A., Qian, X.Y., Zhu, D.C., and Ke, S., 2016, Deep carbon cycle recorded by calcium-silicate rocks (rodingites) in a subduction-related ophiolite: Deep Carbon Cycle Recorded by Rodingite: Geophysical Research Letters, v. 43, p. 11,635-11,643, doi:10.1002/2016GL070474.

Duan, W.-Y., Li, X.-P., Schertl, H.-P., Willner, A.P., Wang, S.-J., Chen, S., and Sun, G.-M., 2022, Rodingitization records from ocean-floor to high pressure metamorphism in the Xigaze ophiolite, southern Tibet: Gondwana Research, v. 104, p. 126–153, doi:10.1016/j.gr.2021.05.013.

Duan, W.-Y., Li, X.-P., Wang, Z.-L., Chen, S., Sun, G.-M., and Zhao, L.-Q., 2021, Thermodynamic modeling and elemental migration for the early stage of rodingitization: An example from the Xialu massif of the Xigaze ophiolite, southern Tibet: Geoscience Frontiers, v. 12, p. 101–125, doi:10.1016/j.gsf.2020.12.006.

Dubińska, E., Bylina, P., Kozłowski, A., Dörr, W., Nejbert, K., Schastok, J., and Kulicki, C., 2004, U–Pb dating of serpentinization: hydrothermal zircon from a metasomatic rodingite shell (Sudetic ophiolite, SW Poland): Chemical Geology, v. 203, p. 183–203, doi:10.1016/j.chemgeo.2003.10.005.

Ferrando, S., Frezzotti, M.L., Orione, P., Conte, R.C., and Compagnoni, R., 2010, Late-Alpine rodingitization in the Bellecombe meta-ophiolites (Aosta Valley, Italian Western Alps): evidence from mineral assemblages and serpentinization-derived $H_2$ -bearing brine: International Geology Review, v. 52, p. 1220–1243, doi:10.1080/00206810903557761.

Fletcher, J.M., Stephens, C.J., Petersen, E.U., and Skerl, L., 1997, Greenschist facies hydrothermal alteration of oceanic gabbros: A case study of element mobility and reaction paths, *in* Karson, J.A., Cannat, M., Miller, D.J., and Elthon, D. eds., Proceedings of the Ocean Drilling Program, 153 Scientific Results, Ocean Drilling Program, Proceedings of the Ocean Drilling Program, v. 153, doi:10.2973/odp.proc.sr.153.1997.

Fouquet, Y. et al., 2010, Geodiversity of hydrothermal processes along the Mid-Atlantic Ridge and ultramafic-hosted mineralization: A new type of oceanic Cu-Zn-Co-Au volcanogenic massive sulfide deposit, *in* Rona, P.A., Devey, C.W., Dyment, J., and Murton, B.J. eds., Diversity of hydrothermal systems on slow spreading ocean ridges, Washington, D. C., American Geophysical Union, Geophysical Monograph Series 188, v. 188, p. 321–367, doi:10.1029/2008GM000746.

Frost, B.R., and Beard, J.S., 2007, On Silica Activity and Serpentinization: Journal of Petrology, v. 48, p. 1351–1368, doi:10.1093/petrology/egm021.

Frost, B.R., Beard, J.S., McCaig, A., and Condliffe, E., 2008, The Formation of Micro-Rodingites from IODP Hole U1309D: Key To Understanding the Process of Serpentinization: Journal of Petrology, v. 49, p. 1579–1588, doi:10.1093/petrology/egn038.

Fukuyama, M., Ogasawara, M., Dunkley, D.J., Wang, K.-L., Lee, D.-C., Hokada, T., Maki, K., Hirata, T., and Kon, Y., 2014, The formation of rodingite in the Nagasaki metamorphic rocks at Nomo Peninsula, Kyushu, Japan - Zircon U-Pb and Hf isotopes and trace element evidence: Formation of rodingite: Island Arc, v. 23, p. 281–298, doi:10.1111/iar.12086.

Groat, L.A., Hawthorne, F.C., and Ercit, T.S., 1992, The chemistry of vesuvianite: The Canadian Mineralogist, v. 30, p. 19–48.

Hatzipanagiotou, K., Tsikouras, B., Migiros, G., Gartzos, E., and Serelis, K., 2003, Origin of rodingites in ultramafic rocks from Lesvos island (NE Aegean, Greece): Ofioliti, v. 28, p. 13–23.

Haws, A.A., Starr, P.G., Dragovic, B., Scambelluri, M., Belmonte, D., Caddick, M.J., Broadwell, K.S., Ague, J.J., and Baxter, E.F., 2021, Meta-rodingite dikes as recorders of subduction zone

metamorphism and serpentinite dehydration: Voltri Ophiolite, Italy: Chemical Geology, v. 565, p. 120077, doi:10.1016/j.chemgeo.2021.120077.

Helgeson, H.C., 1969, Thermodynamics of hydrothermal systems at elevated temperatures and pressures: American Journal of Science, v. 267, p. 729–804, doi:10.2475/ajs.267.7.729.

Honnorez, J., and Kirst, P., 1975, Petrology of rodingites from the equatorial Mid-Atlantic fracture zones and their geotectonic significance: Contributions to Mineralogy and Petrology, v. 49, p. 233–257, doi:10.1007/BF00376590.

Hu, C.-N., and Santosh, M., 2018, Devonian rodingite from the northern margin of the North China Craton: mantle wedge metasomatism during ocean-continent convergence: International Geology Review, v. 60, p. 1073–1097, doi:10.1080/00206814.2017.1365631.

Janecky, D.R., and Seyfried, W.E., 1983, The solubility of magnesium-hydroxide-sulfate-hydrate in seawater at elevated temperatures and pressures: American Journal of Science, v. 283, p. 831–860, doi:10.2475/ajs.283.8.831.

Karkalis, C., Magganas, A., Koutsovitis, P., Pomonis, P., and Ntaflos, T., 2022, Multiple Rodingitization Stages in Alkaline, Tholeiitic, and Calc-Alkaline Basaltic Dikes Intruding Exhumed Serpentinized Tethyan Mantle from Evia Island, Greece (S. Ao, Ed.): Lithosphere, v. 2022, p. 9507697, doi:10.2113/2022/9507697.

Katoh, T., and Niida, K., 1983, Rodingites from the Kamuikotan Tectonic Belt, Hokkaido: Journal of Faculty of Science, Hokkaido University, p. 151–169.

Kelley, D.S. et al., 2001, An off-axis hydrothermal vent field near the Mid-Atlantic Ridge at 30° N: Nature, v. 412, p. 145–149, doi:10.1038/35084000.

Klein, F., Grozeva, N.G., Seewald, J.S., McCollom, T.M., Humphris, S.E., Moskowitz, B., Berquó, T.S., and Kahl, W.-A., 2015, Experimental constraints on fluid-rock reactions during incipient serpentinization of harzburgite†: American Mineralogist, v. 100, p. 991–1002, doi:10.2138/am-2015-5112.

Kobayashi, S., and Kaneda, H., 2010, Rodingite with Ti- and Cr-rich vesuvianite from the Sartuohai chromium deposit, Xinjiang, China: Journal of Mineralogical and Petrological Sciences, v. 105, p. 112–122, doi:10.2465/jmps.081224.

Koutsovitis, P., Magganas, A., Pomonis, P., and Ntaflos, T., 2013, Subduction-related rodingites from East Othris, Greece: Mineral reactions and physicochemical conditions of formation: Lithos, v. 172–173, p. 139–157, doi:10.1016/j.lithos.2013.04.009.

Laborda-López, C., López-Sánchez-Vizcaíno, V., Marchesi, C., Gómez-Pugnaire, M.T., Garrido, C.J., Jabaloy-Sánchez, A., Padrón-Navarta, J.A., and Hidas, K., 2018, High- *P* metamorphism of rodingites during serpentinite dehydration (Cerro del Almirez, Southern Spain): Implications for the redox state in subduction zones: Journal of Metamorphic Geology, v. 36, p. 1141–1173, doi:10.1111/jmg.12440.

Laborda-López, C., Marchesi, C., López Sánchez-Vizcaíno, V., Gómez-Pugnaire, M.T., Dale, C.W., Jabaloy-Sánchez, A., Padrón-Navarta, J.A., Román-Alpiste, M.J., and Garrido, C.J., 2020, Geochemical evolution of rodingites during subduction: insights from Cerro del Almirez (southern Spain): Lithos, v. 370–371, p. 105639, doi:10.1016/j.lithos.2020.105639.

Li, X.-P., Duan, W.-Y., Zhao, L.-Q., Schertl, H.-P., Kong, F.-M., Shi, T.-Q., and Zhang, X., 2017, Rodingites from the Xigaze ophiolite, southern Tibet – new insights into the processes of rodingitization: European Journal of Mineralogy, v. 29, p. 821–837, doi:10.1127/ejm/2017/0029-2633.

Li, X.-P., Rahn, M., and Bucher, K., 2008, Eclogite facies metarodingites – phase relations in the system $SiO_2$-$Al_2O_3$-$Fe_2O_3$-FeO-MgO-CaO-$CO_2$-$H_2O$: an example from the Zermatt-Saas ophiolite: Journal of Metamorphic Geology, v. 26, p. 347–364, doi:10.1111/j.1525-1314.2008.00761.x.

Li, X.-P., Rahn, M., and Bucher, K., 2004, Metamorphic Processes in Rodingites of the Zermatt-Saas Ophiolites: International Geology Review, v. 46, p. 28–51, doi:10.2747/0020-6814.46.1.28.

Li, X.-P., Zhang, L., Wei, C., Ai, Y., and Chen, J., 2007, Petrology of rodingite derived from eclogite in western Tianshan, China: Journal of Metamorphic Geology, v. 25, p. 363–382, doi:10.1111/j.1525-1314.2007.00700.x.

MacLeod, C.J., Dick, H.J., and Blum, P., 2017, Site U1473, *in* Proceedings of the International Ocean Discovery Program, International Ocean Discovery Program, Proceedings of the International Ocean Discovery Program 360, doi:10.14379/iodp.proc.360.2017.

Mittwede, S.K., and Schandl, E.S., 1992, Rodingites from the southern Appalachian Piedmont, South Carolina, USA: European Journal of Mineralogy, v. 4, p. 7–16, doi:10.1127/ejm/4/1/0007.

Mottl, M.J., 1983, Metabasalts, axial hor springs, and the structure of hydrothermal systems at mid-ocean ridges: Geological Society of America Bulletin, v. 94, p. 161–180.

Mubarak, H.S., Azer, M.K., Surour, A.A., Moussa, H.E., Asimow, P.D., and Kabesh, M.M.L., 2020, Mineralogical and geochemical study of rodingites and associated serpentinized peridotite, Eastern Desert of Egypt, Arabian-Nubian Shield: Lithos, v. 374–375, p. 105720, doi:10.1016/j.lithos.2020.105720.

Murzin, V.V., and Shanina, S.N., 2007, Fluid regime and origin of gold-bearing rodingites from the Karabash alpine-type ultrabasic massif, Southern Ural: Geochemistry International, v. 45, p. 998–1011, doi:10.1134/S0016702907100047.

Nishiyama, T., Yoshida-Shiosaki, C., Mori, Y., and Shigeno, M., 2017, Interplay of irreversible reactions and deformation: a case of hydrofracturing in the rodingite-serpentinite system: Progress in Earth and Planetary Science, v. 4, p. UNSP 1, doi:10.1186/s40645-016-0115-4.

Nordstrom, D.K. et al., 1979, A comparison of computerized chemical models for equilibrium calculations in aqueous species, *in* Chemical Modeling in aqueous systems, speciation, sorption, solubility and kinetics, American Chemical Society, p. 857–892.

Normand, C., 2001, Experimental and Field Investigations of Serpentinization and Rodingitization. [PhD.]: Department of Earth and Planetary Sciences, McGill University.

Normand, C., and Williams-Jones, A.E., 2007, Physicochemical conditions and timing of rodingite formation: evidence from rodingite-hosted fluid inclusions in the JM Asbestos mine, Asbestos, Québec: Geochemical Transactions, v. 8, p. 11, doi:10.1186/1467-4866-8-11.

O'Hanley, D.S., Schandl, E.S., and Wicks, F.J., 1992, The origin of rodingites from Cassiar, British Columbia, and their use to estimate T and P (H20) during serpentinization: Geochimica et Cosmochimica Acta, v. 56, p. 97–108.

Palandri, J.L., and Reed, M.H., 2004, Geochemical models of metasomatism in ultramafic systems: serpentinization, rodingitization, and sea floor carbonate chimney precipitation: Geochimica et Cosmochimica Acta, v. 68, p. 1115–1133, doi:10.1016/j.gca.2003.08.006.

Parkhurst, D.L., and Appelo, C.A.J., 2013, Description of Input and Examples for PHREEQC Version 3—A Computer Program for Speciation, Batch-Reaction, One-Dimensional Transport, and Inverse Geochemical Calculations., *in* Techniques and Methods 6–A43, U.S. Geological Survey, Techniques and Methods.

Peng, D.-Y., and Robinson, D.B., 1976, A New Two-Constant Equation of State: Industrial & Engineering Chemistry Fundamentals, v. 15, p. 59–64, doi:10.1021/i160057a011.

Puschnig, A.R., 2002, Metasomatic alterations at mafic-ultramafic contacts in Valmalenco (Rhetic Alps, N-Italy): Schweizerische mineralogische und petrographische Mitteilungen, v. 82, p. 515–536.

Rice, J.M., 1983, Metamorphism of rodingites: part I. Phase relations in a portion of the system CaO-MgO-Al2O3-SiO2-CO2-H2O.: American Journal of Science, v. 283 A, p. 121–150.

Rogkala, A., Petrounias, P., Koutsovitis, P., Giannakopoulou, P.P., Pomonis, P., Lampropoulou, P., and Hatzipanagiotou, K., 2022, Rodingites from the Veria-Naousa ophiolite (Greece): Mineralogical evolution, metasomatism and petrogenetic processes: Geochemistry, p. 125860, doi:10.1016/j.chemer.2021.125860.

Rouméjon, S., Cannat, M., Agrinier, P., Godard, M., and Andreani, M., 2015, Serpentinization and Fluid Pathways in Tectonically Exhumed Peridotites from the Southwest Indian Ridge (62–65°E): Journal of Petrology, v. 56, p. 703–734, doi:10.1093/petrology/egv014.

Rouméjon, S., Williams, M.J., and Früh-Green, G.L., 2018, In-situ oxygen isotope analyses in serpentine minerals: Constraints on serpentinization during tectonic exhumation at slow- and ultraslow-spreading ridges: Lithos, v. 323, p. 156–173, doi:10.1016/j.lithos.2018.09.021.

Salvioli-Mariani, E., Boschetti, T., Toscani, L., Montanini, A., Petriglieri, J.R., and Bersani, D., 2020, Multi-stage rodingitization of ophiolitic bodies from Northern Apennines (Italy): Constraints from petrography, geochemistry and thermodynamic modelling: Geoscience Frontiers, v. 11, p. 2103–2125, doi:10.1016/j.gsf.2020.04.017.

Schandl, E.S., O'Hanley, D.S., and Wicks, F.J., 1989, Rodingites in serpentinized ultramafic rocks of the Abitibi Greenstone belt, Ontario: Canadian Mineralogist, v. 27, p. 579–591.

Schandl, E.S., O'Hanley, D.S., Wicks, F.J., and Kyser, T.K., 1990, Fluid inclusions in rodingite; a geothermometer for serpentinization: Economic Geology, v. 85, p. 1273–1276, doi:10.2113/gsecongeo.85.6.1273.

Seyfried, W.E., Berndt, M.E., and Seewald, J.S., 1998, Hydrothermal alteration processes at mid-ocean ridges: contraints from diabase alteration experiments, hot-spring lfuids and composition of the oceanic crust: Canadian Mineralogist, v. 26, p. 187–804.

Seyfried, W.E., and Bischoff, J.L., 1981, Experimental seawater-basalt interaction at 300°C, 500 bars, chemical exchange, secondary mineral gromation and implications for the transport of heavy metals: Geochimica et Cosmochimica Acta, v. 45, p. 135–147.

Seyfried, W.E., Foustoukos, D.I., and Fu, Q., 2007, Redox evolution and mass transfer during serpentinization: An experimental and theoretical study at 200°C, 500bar with implications

for ultramafic-hosted hydrothermal systems at Mid-Ocean Ridges: Geochimica et Cosmochimica Acta, v. 71, p. 3872–3886, doi:10.1016/j.gca.2007.05.015.

Seyfried, W.E., Pester, N.J., Tutolo, B.M., and Ding, K., 2015, The Lost City hydrothermal system: Constraints imposed by vent fluid chemistry and reaction path models on subseafloor heat and mass transfer processes: Geochimica et Cosmochimica Acta, v. 163, p. 59–79, doi:10.1016/j.gca.2015.04.040.

Tang, Y., Zhai, Q.-G., Hu, P.-Y., Wang, J., Xiao, X.-C., Wang, H.-T., Tang, S.-H., and Lei, M., 2018, Rodingite from the Beila ophiolite in the Bangong–Nujiang suture zone, northern Tibet: New insights into the formation ofophiolite-related rodingite: Lithos, v. 316–317, p. 33–47, doi:10.1016/j.lithos.2018.07.006.

Tsikouras, B., Karipi, S., and Hatzipanagiotou, K., 2013, Evolution of rodingites along stratigraphic depth in the Iti and Kallidromon ophiolites (Central Greece): Lithos, v. 175–176, p. 16–29, doi:10.1016/j.lithos.2013.04.021.

Wang, S., Li, X.-P., Duan, W., Kong, F., and Wang, Z., 2019, Record of Early-Stage Rodingitization from the Purang Ophiolite Complex, Western Tibet: Journal of Earth Science, v. 30, p. 1108–1124, doi:10.1007/s12583-019-1244-7.

Wetzel, L.R., and Shock, E.L., 2000, Distinguishing ultramafic-from basalt-hosted submarine hydrothermal systems by comparing calculated vent fluid compositions: Journal of Geophysical Research: Solid Earth, v. 105, p. 8319–8340, doi:10.1029/1999JB900382.

Xiong, J.-W., Chen, Y.-X., Scambelluri, M., Qiao, X.-Y., Chen, Y., Huang, F., Belmonte, D., and Zhao, Z.-F., 2024, Fluid-metasomatized rocks with extremely low δ26Mg values in subducted oceanic lithosphere: Implications for mantle Mg isotope heterogeneity and the origin of low-δ26Mg magmas: Geochimica et Cosmochimica Acta, v. 371, p. 111–125, doi:10.1016/j.gca.2024.03.006.

Zanoni, D., Rebay, G., and Spalla, M.I., 2016, Ocean floor and subduction record in the Zermatt-Saas rodingites, Valtournanche, Western Alps: Journal of Metamorphic Geology, v. 34, p. 941–961, doi:10.1111/jmg.12215.

Zhang, G., Lu, P., Zhang, Y., Tu, K., and Zhu, C., 2020, SupPhreeqc: A program for generating customized Phreeqc thermodynamic datasets from Supcrtbl and extending calculations to elevated pressures and temperatures: Computers & Geosciences, v. 143, p. 104560, doi:10.1016/j.cageo.2020.104560.

Zhao, M.-S., Chen, Y.-X., Xiong, J.-W., Qiao, X.-Y., Zheng, Y.-F., Duan, W.-Y., Huang, F., and Zhao, Z.-F., 2023, Magnesium–oxygen isotope constraints on the origin of rodingites in oceanic lithosphere: Chemical Geology, v. 635, p. 121612, doi:10.1016/j.chemgeo.2023.121612.

Zimmer, K., Zhang, Y., Lu, P., Chen, Y., Zhang, G., Dalkilic, M., and Zhu, C., 2016, SUPCRTBL: A revised and extended thermodynamic dataset and software package of SUPCRT92: Computers & Geosciences, v. 90, p. 97–111, doi:10.1016/j.cageo.2016.02.013.